nature climate change

LETTERS

PUBLISHED ONLINE: 24 APRIL 2017 | DOI: 10.1038/NCLIMATE3277

Weakening temperature control on the interannual variations of spring carbon uptake across northern lands

Shilong Piao[1,2,3]*, Zhuo Liu[2], Tao Wang[1,3], Shushi Peng[2], Philippe Ciais[4], Mengtian Huang[2], Anders Ahlstrom[5], John F. Burkhart[6], Frédéric Chevallier[4], Ivan A. Janssens[7], Su-Jong Jeong[8], Xin Lin[4], Jiafu Mao[9], John Miller[10,11], Anwar Mohammat[12], Ranga B. Myneni[13], Josep Peñuelas[14,15], Xiaoying Shi[9], Andreas Stohl[16], Yitong Yao[2], Zaichun Zhu[2] and Pieter P. Tans[10]

Ongoing spring warming allows the growing season to begin earlier, enhancing carbon uptake in northern ecosystems[1–3]. Here we use 34 years of atmospheric CO_2 concentration measurements at Barrow, Alaska (BRW, 71° N) to show that the interannual relationship between spring temperature and carbon uptake has recently shifted. We use two indicators: the spring zero-crossing date of atmospheric CO_2 (SZC) and the magnitude of CO_2 drawdown between May and June (SCC). The previously reported strong correlation between SZC, SCC and spring land temperature (ST) was found in the first 17 years of measurements, but disappeared in the last 17 years. As a result, the sensitivity of both SZC and SCC to warming decreased. Simulations with an atmospheric transport model[4] coupled to a terrestrial ecosystem model[5] suggest that the weakened interannual correlation of SZC and SCC with ST in the last 17 years is attributable to the declining temperature response of spring net primary productivity (NPP) rather than to changes in heterotrophic respiration or in atmospheric transport patterns. Reduced chilling during dormancy and emerging light limitation are possible mechanisms that may have contributed to the loss of NPP response to ST. Our results thus challenge the 'warmer spring–bigger sink' mechanism.

For the past decade, boreal forests have been a net carbon sink[6]; but the sink-or-source status of arctic tundra cannot be deduced from current observations[7]. Both modelling and observational studies have shown that spring warming has advanced leaf onset in the Northern Hemisphere, thus lengthening the photosynthesis season and, in turn, strengthening net carbon uptake[1–3,8]. The effect of temperature on spring CO_2 uptake by plants has been identified as the main mechanism explaining the year-to-year variations of atmospheric CO_2 in spring. For instance, at Point Barrow (hereafter referred to as Barrow) atmospheric measurement station in north Alaska, the periodical spring drawdown of atmospheric CO_2 occurs earlier in the year when spring temperature is warmer[1,9]. Beyond the rather well-studied interannual variations, examples of decadal changes in climate affecting ecosystems remain elusive. Limited evidence from tree-ring data[10] and satellite vegetation greenness[11,12] does give hints that the response of northern terrestrial carbon fluxes to temperature may not be constant over timescales of decades.

Here, we investigate changes in the interannual relationship between spring temperature and CO_2 uptake by northern ecosystems (NEP, net ecosystem productivity) over the past three decades. We use: the longest high-latitude atmospheric CO_2 record from Barrow; the LMDZ4 (Laboratoire de Météorologie Dynamique, 'Z' stands for zoom) atmospheric transport model[4] simulating CO_2 concentrations from NEP produced by the process-based terrestrial carbon model ORCHIDEE[5] (ORganizing Carbon and Hydrology In Dynamic Ecosystems), which also allows the partitioning of NEP into its component fluxes of NPP and heterotrophic respiration (HR); and satellite observations of vegetation greenness, a proxy for photosynthesis. Temporal variations in the seasonal variability of CO_2 in spring at Barrow reflect changes in northern NEP and atmospheric mixing[1,13]. We consider two indicators of spring CO_2 variations at Barrow, namely the SZC (the day of year when CO_2 crosses down through its annual mean level; Supplementary Figs 1 and 2a) and the SCC (spring carbon capture, the seasonal magnitude of the observed CO_2 decrease between the first week of May and the last week of June; Supplementary Figs 1 and 2b)[1,13,14]. These two indicators are correlated with land temperature to give the response of spring NEP to temperature (all variables are detrended, see Methods).

[1]Key Laboratory of Alpine Ecology and Biodiversity, Institute of Tibetan Plateau Research, Chinese Academy of Sciences, Beijing 100085, China. [2]Sino-French Institute for Earth System Science, College of Urban and Environmental Sciences, Peking University, Beijing 100871, China. [3]Center for Excellence in Tibetan Earth Science, Chinese Academy of Sciences, Beijing 100085, China. [4]Laboratoire des Sciences du Climat et de l'Environnement, CEA CNRS UVSQ, Gif-sur-Yvette 91191, France. [5]School of Earth, Energy and Environmental Sciences, Stanford University, Stanford, California 94305-2210, USA. [6]Department of Geosciences, University of Oslo, PO Box 1047 Blindem, 0316 Oslo, Norway. [7]Department of Biology, University of Antwerp, Universiteitsplein 1, 2610 Wilrijk, Belgium. [8]School of Environmental Science and Engineering, South University of Science and Technology of China, Shenzhen 518055, China. [9]Climate Change Science Institute and Environmental Sciences Division, Oak Ridge National Laboratory, Oak Ridge, Tennessee 37831, USA. [10]National Oceanic and Atmospheric Administration Earth Systems Research Laboratory (NOAA/ESRL), 325 Broadway, Boulder, Colorado 80305, USA. [11]Cooperative Institute for Research in Environmental Sciences, University of Colorado, Boulder 80309, USA. [12]Xinjiang Institute of Ecology and Geography, Chinese Academy of Sciences, Urumqi 830011, Xinjiang, China. [13]Department of Earth and Environment, Boston University, 675 Commonwealth Avenue, Boston, Massachusetts 02215, USA. [14]CREAF, Cerdanyola del Valles, Barcelona 08193, Catalonia, Spain. [15]CSIC, Global Ecology Unit CREAF-CEAB-CSIC-UAB, Cerdanyola del Valles, Barcelona 08193, Catalonia, Spain. [16]NILU—Norwegian Institute for Air Research, PO Box 100, 2027 Kjeller, Norway. *e-mail: slpiao@pku.edu.cn

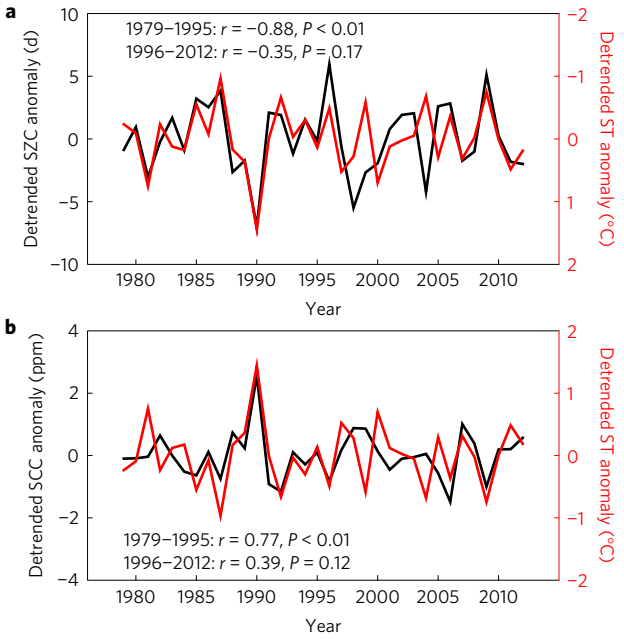

Figure 1 | Time series of detrended anomalies. a, SZC (black) and ST (red). **b**, SCC (black) and ST (red). Interannual correlation coefficients of SZC and SCC with ST during the first 17 years (1979–1995) and the last 17 years (1996–2012) are inset as (*r*). Note that we have reversed the scale of ST in **a** for a better visual effect.

The average spring temperature from March to June (ST) over vegetated land north of 50° N was used, since this time period shows the strongest negative interannual correlation between ST and SZC, and the strongest positive interannual correlation with SCC (Supplementary Fig. 3).

All variables are detrended in the statistical correlation analysis since we focus on the interannual relationship between spring carbon uptake and temperature (see Methods). As shown in Figs 1a and 2a, the interannual relationship between SZC and ST is not stable over the full length of the Barrow record. Partial correlations remove the statistical influence of other climatic variables that co-vary with ST and may affect NEP, and in turn atmospheric CO_2—in particular precipitation and radiation (here approximated by cloudiness). We found that the partial correlation between SZC and ST (R_{SZC}) was −0.84 during the period 1979–1995, but decreased to −0.11 during the period 1996–2012. Robustness tests randomly selecting 14 years in the first period (number of degrees of freedom = 10) showed that all combinations of years give a statistically significant negative R_{SZC} ($P < 0.05$) during the first period, whereas only 2% of the combinations produce (marginally) significant negative R_{SZC} ($P < 0.10$) during the second period (Fig. 2a). Partial correlations of SZC and SCC with spring cloudiness and precipitation are not significant for either period (Supplementary Fig. 4).

The sensitivity of SZC to ST was determined using multiple linear regressions with ST, precipitation and cloudiness. The sensitivity of SZC to ST, hereafter called γ_{SZC}, is the slope of the regression between SZC and ST, with both variables detrended (Supplementary Fig. 5a). The value of γ_{SZC} is negative since warmer years are associated with an advance of SZC. Like partial correlations between ST and SZC, γ_{SZC} significantly decreased, that is, became less negative, in the second period relative to the first period (based on two-sample *t*-test, $P < 0.05$) (see Supplementary Fig. 5a). This decrease in γ_{SZC} occurs in parallel with the loss of interannual correlation between SZC and ST in the second period. Performing the same analysis using SCC instead of SZC produces similar results, with a decrease of γ_{SCC} (Figs 1b and 2b and Supplementary Fig. 5b).

To investigate whether the decrease in R_{SZC} and R_{SCC} could be explained by a change in the NEP flux area influencing the spring drawdown of CO_2 at Barrow—that is, the atmospheric footprint of the station—we calculated the main footprint area, which is mainly in eastern Siberia and Alaska (see Methods and Supplementary Fig. 6). Using climate variables averaged only over the main footprint area where NEP impacts the CO_2 drawdown measured at Barrow, we also found a decline in R_{SZC} and R_{SCC} (see Methods and Supplementary Fig. 7). Climate observations are scarce at high latitudes; thus, to test if the decline of R_{SZC} and R_{SCC} is robust to the choice of a climate forcing data set, we used different products (Supplementary Fig. 8). We also adopted different parameters for atmospheric CO_2 data processing (see Methods and Supplementary Fig. 9), changed the duration of the period before June over which ST is averaged (see Methods, Supplementary Fig. 9), used weekly instead of daily CO_2 data from Barrow (Supplementary Fig. 10), and tried to include co-variation in snow water equivalent[15] as well as previous winter temperature in the partial correlation analysis (Supplementary Fig. 11). All these tests confirmed that the decrease of R_{SZC} and R_{SCC} over time is a robust finding. Two other long-term northern CO_2 records from the Alaskan station at Cold Bay and the Norwegian Ocean Station M also show a similar decrease of R_{SZC} and R_{SCC}, albeit with a generally weaker interannual correlation between CO_2 and ST at Station M compared to Barrow (Supplementary Fig. 12). Finally, the decrease of R_{SZC} and R_{SCC} at Barrow did not depend on the precise duration of the first and second periods (Supplementary Fig. 13).

We tested the following hypotheses to explain the decrease of R_{SZC} and γ_{SZC}: (H1a) spring NEP which controls the timing and magnitude of spring CO_2 drawdown at Barrow, shows a decreasing sensitivity to ST because NPP is becoming less sensitive to temperature, while the sensitivity of HR is stable; (H1b) HR is becoming more sensitive to temperature, while the sensitivity of NPP is stable; (H2) the decrease of R_{SZC} and γ_{SZC} are not due to a changing response of NEP to ST, but reflect changes in atmospheric transport.

To test these hypotheses, we performed factorial simulations with the atmospheric transport model LMDZ4[4], coupled with the spatially and temporally explicit ecosystem model of NEP, ORCHIDEE[5]. The transport model can be run with year-to-year varying winds over the past 34 years (Table 1). Daily NEP from the ecosystem model forced by historical climate[16] and rising atmospheric CO_2 (ref. 5) was prescribed to the transport model to simulate CO_2 at Barrow during 1979–2012 (see Methods). The version of ORCHIDEE used here does not include permafrost dynamics such as soil thaw[17] and disturbances such as fire. The factorial simulations (Table 1) include year-to-year varying atmospheric transport applied to either year-to-year varying NEP (TFTT) or periodical (with the same seasonal cycle each year) NEP (CFTT). See Table 1 for explanation of abbreviations. In addition, we performed runs where NEP was set to be year-to-year varying in boreal regions (>50° N) only and periodical elsewhere (TFTT-B). The contribution of year-to-year varying NEP to SZC and SCC at Barrow is diagnosed from the difference in the simulated CO_2 concentration between TFTT and CFTT (referred to as TFCT). The specific contribution of boreal ecosystem NEP is obtained from the difference in CO_2 between TFTT-B and CFTT (referred to as TFCT-B). This latter diagnostic shows that, consistent with ref. 18, SZC and SCC variations at Barrow are dominated by NEP fluctuations in boreal ecosystems (Supplementary Fig. 14). The observed weakening of R_{SZC} (Fig. 2a and Supplementary Fig. 13a) is captured by both simulations TFCT and TFCT-B, indicating that the ORCHIDEE model has some ability to capture the changing response of NEP to ST over the past 34 years. Further, the consistency between TFCT and TFCT-B implies that changes in NEP from boreal regions rather than from temperate and subtropical regions are mainly responsible for the observed weakening in R_{SZC}. Varying atmospheric transport does not seem to play an

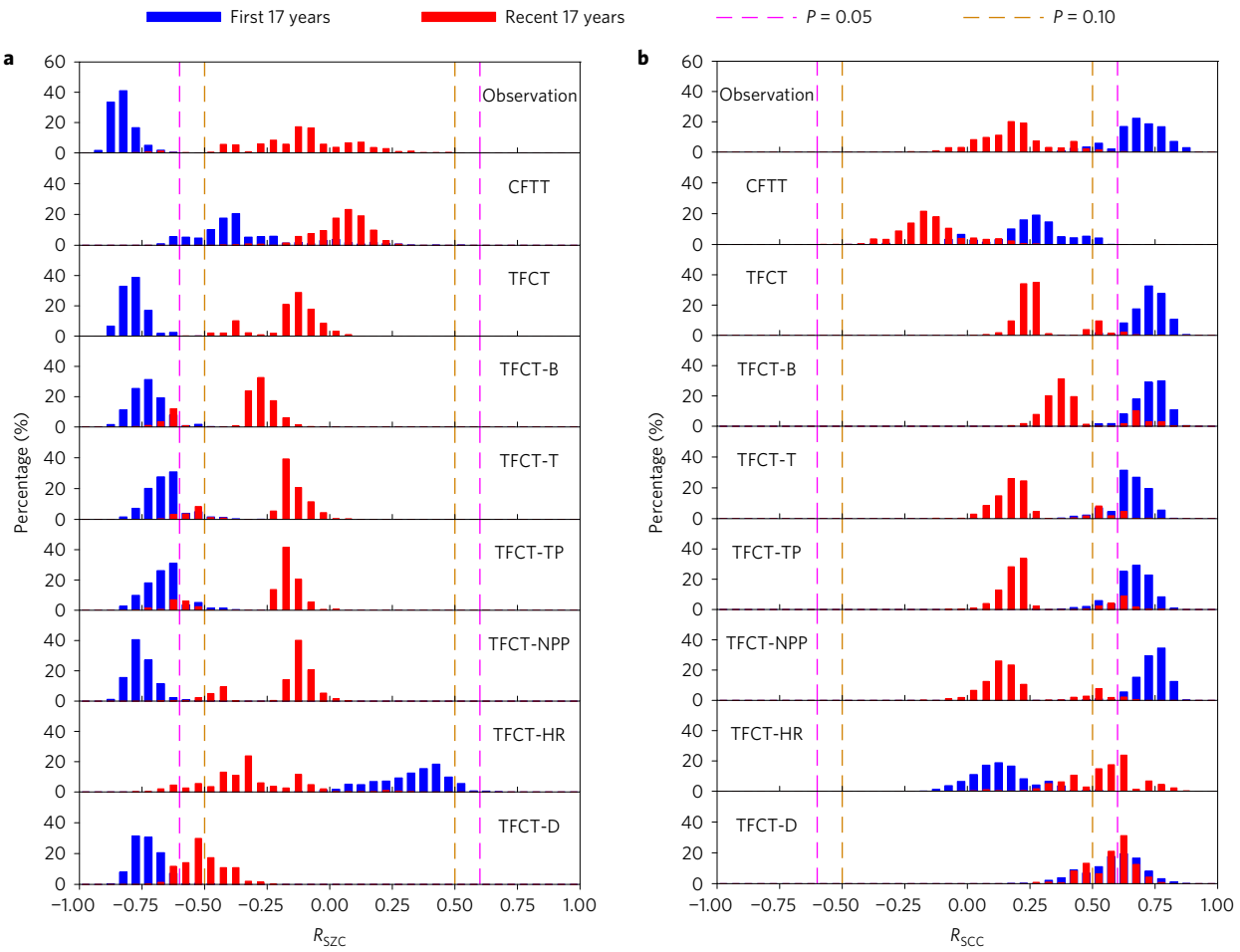

Figure 2 | The partial correlation coefficient of spring carbon uptake and temperature during different periods. a,**b**, Frequency distributions of the partial correlation coefficient of SZC (R_{SZC}) (**a**) and SCC (R_{SCC}) (**b**) with March–June temperature during the first 17 years (1979–1995) and the second, more recent 17 years (1996–2012). Frequency distributions of the partial correlation coefficient of SZC (R_{SZC}) (**a**) and SCC (R_{SCC}) (**b**) with March–June temperature during the first 17 years (1979–1995, blue) and the recent 17 years (1996–2012, red). Statistically significant partial correlation coefficients are indicated as dotted lines (magenta: $P < 0.05$ and brown: $P < 0.1$). All variables were detrended for each study period before partial correlation analysis. Abbreviations of transport simulations are defined in Table 1. CFTT indicates the effect of wind change on R_{SZC} and R_{SCC}; TFCT indicates the effect of global NEP change on R_{SZC} and R_{SCC}; TFCT-B indicates the effect of boreal NEP change on R_{SZC} and R_{SCC}; TFCT-T indicates the effect of change in boreal NEP only driven by temperature on R_{SZC} and R_{SCC}; TFCT-TP indicates the effect of change in boreal NEP driven by both temperature and precipitation on R_{SZC} and R_{SCC}; TFCT-NPP indicates the effect of boreal NPP change on R_{SZC} and R_{SCC}; TFCT-HR indicates the effect of boreal HR change on R_{SZC} and R_{SCC}; TFCT-D indicates the effect of change in temperature during the dormancy period only (November–April) on R_{SZC} and R_{SCC}.

important role in the changing interannual correlation between SZC and ST because the simulation with periodical NEP and year-to-year varying transport (CFTT) produced no significant change in interannual correlation, as measured by R_{SZC} (Fig. 2a and Supplementary Fig. 13a). We obtained similar results looking at SCC instead of SZC at Barrow (Fig. 2b and Supplementary Fig. 13b). In summary, these simulation results are consistent with both hypothesis H1a and H1b, but falsify H2 because NEP changes over boreal regions rather than transport changes explained the loss of interannual correlation between ST and SZC over time. In addition, we also found negligible contributions from variation in air–sea CO_2 fluxes to the decline in R_{SZC} or R_{SCC} (see Methods and Supplementary Fig. 15).

To attribute simulated R_{SZC} and R_{SCC} changes to temperature versus precipitation effects on NEP, we performed two additional simulations: TFCT-T where only historical temperature was varied and precipitation as well as other climate drivers of the ORCHIDEE ecosystem model are periodical; and TFCT-TP where both historical temperature and precipitation were varied (see Methods and Table 1). Atmospheric CO_2 simulated with only historical temperature impacting NEP, reproduced a decrease of R_{SZC} and γ_{SZC} at Barrow (Fig. 2a and Supplementary Fig. 5a). Further, the simulated decrease of R_{SZC} in TFCT-T was close to the one found in TFCT-B where all historical climate drivers were varied (Supplementary Fig. 13a). This suggests that the decrease of R_{SZC} and γ_{SZC} is mainly attributable to changes in the temperature response of NEP in boreal regions (see also Fig. 2b and Supplementary Fig. 5b for SCC).

In the terrestrial ecosystem model used in this study (ORCHIDEE), interannual variations of spring NEP are mainly explained by NPP variations rather than variations in HR (Supplementary Fig. 16). As a further test of H1a against H1b, we performed two additional transport simulations where HR was set to be periodical and NPP was year-to-year varying (TFCT-NPP), and vice versa (TFCT-HR) (see Methods and Table 1). The results shown in Fig. 2 indicate that the simulated decrease of R_{SZC} and R_{SCC}, which matches the observed decrease, is mainly due to a loss of interannual correlation between NPP and ST (see also Supplementary Fig. 13). This favours hypothesis H1a over H1b, although this result should be reproduced in the future by alternative sets of NPP and HR from terrestrial ecosystem models.

Table 1 | Summary of transport simulations performed.

Simulation name	Abbreviation	Carbon flux	Wind
Constant Flux (NEP) with Transient Transport	CFTT	Periodical NEP of 1979 from ORCHIDEE simulation S3 where both CO_2 and all historical climate variables are varied	vary
Transient Flux (NEP) with Transient Transport	TFTT	Year-to-year varying NEP from simulation S3 where both CO_2 and all historical climate variables are varied	vary
Transient Boreal Flux (NEP) with Transient Transport	TFTT-B	Year-to-year varying NEP in boreal regions (north of 50° N) and periodical NEP of 1979 elsewhere	vary
Transient Flux (NEP) with Transient Transport under scenario with varied Temperature	TFTT-T	The same as TFTT-B, but NEP from simulation S1 where only historical temperature is varied	vary
Transient Flux (NEP) with Transient Transport under scenario with varied Temperature and Precipitation	TFTT-TP	The same as TFTT-B, but NEP from simulation S2 where both historical temperature and precipitation are varied	vary
Transient Flux (NPP) with Transient Transport	TFTT-NPP	Year-to-year varying NPP and periodical HR of 1979 in boreal regions	vary
Transient Flux (HR) with Transient Transport	TFTT-HR	Year-to-year varying HR and periodical NPP of 1979 in boreal regions	vary
Transient Flux (NEP) with Transient Transport under scenario with varied temperature from May to October	TFTT-D	The same as TFTT-B, but NEP from simulation S4 where only historical temperature from May to October is varied	vary
Transient TEmperate Flux (NEP) with Transient Transport	TFTT-TE	Year-to-year varying NEP in temperate regions (30° N–50° N) and periodical NEP of 1979 elsewhere	vary

TFCT = TFTT–CFTT, indicating the effect of global NEP change. TFCT-B = TFTT-B–CFTT, indicating the effect of boreal NEP change. TFCT-T = TFTT-T–CFTT, indicating the effect of boreal NEP change driven by only historical temperature change. TFCT-TP = TFTT-TP–CFTT, indicating the effect of boreal NEP change driven by both historical temperature and precipitation change. TFCT-NPP = TFTT-NPP–CFTT, indicating the effect of boreal NPP change. TFCT-HR = TFTT-HR–CFTT, indicating the effect of boreal HR change. TFCT-D = TFTT-T–TFTT-D, indicating the effect of boreal NEP change driven by only historical temperature change during the dormancy period. TFCT-TE = TFTT-TE–CFTT, indicating the effect of temperate NEP change.

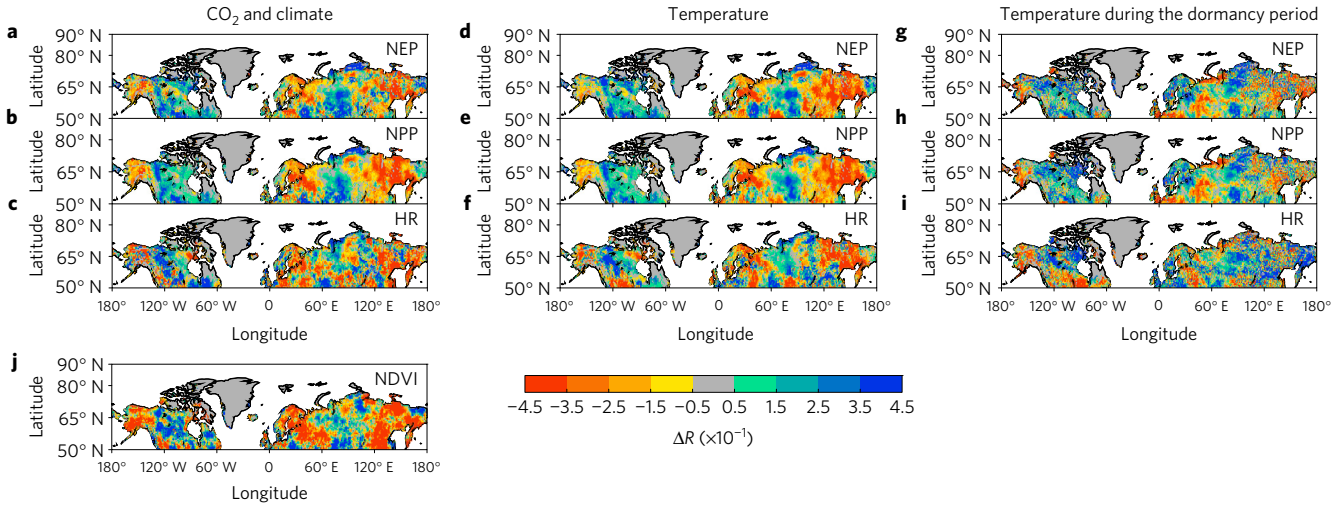

Figure 3 | Spatial distribution of difference in average partial correlation coefficient of spring carbon flux (NEP, NPP and HR) and NDVI with March–June temperature between 1996–2012 and 1979–1995. The partial correlation coefficient is calculated by statistically controlling for interannual variation in precipitation and cloud cover from March to June. Here we compute the spring carbon flux as the total flux from May to June. Carbon fluxes are derived from ORCHIDEE simulations S3 where atmospheric CO_2 and all historical climatic factors were changed (**a**–**c**), from simulation S1 where only historical temperature was changed (**d**–**f**), and from the difference between simulation S1 and S4 where only historical temperature from May to October was changed (**g**–**i**). For each grid, we calculate the partial correlation coefficient through randomly selecting 14 years in the periods of 1979–1995 and 1996–2012, and then taking the mean value for the corresponding period. Only gridded pixels with statistically significant difference at 95% ($P < 0.05$) level are shown. Note that NDVI data (**j**) are only available from 1982 to 2011, so in this case we calculate the partial correlation coefficient through randomly selecting 12 years among 1982–1996 and 1997–2011. All variables are detrended for each study period before partial correlation analysis.

Finally, we examined the spatial distribution of changes in the partial correlation coefficient between ST and NEP ($R_{\text{NEP-T}}$) simulated by ORCHIDEE during the past three decades (Fig. 3). The main footprint region of NEP fluxes influencing the Barrow CO_2 drawdown in spring is Alaska and eastern Siberia (Supplementary Fig. 6). In these two regions, we found a significant decrease in the local $R_{\text{NEP-T}}$ according to ORCHIDEE simulations (Fig. 3a), resulting from a decrease in the interannual correlation between ST and NPP ($R_{\text{NPP-T}}$) (Fig. 3b). Similar spatial patterns of change in $R_{\text{NPP-T}}$ also emerge from the analysis of long-term time series of the Normalized Difference Vegetation Index (NDVI) data, a proxy for vegetation photosynthesis which is related to NPP (see Fig. 3j and Supplementary Fig. 17). This suggests that the decrease in the partial correlation between SZC, SCC and ST at Barrow is unlikely to be due to changes in the spatial coherence of temperature variation. In addition to Alaska and eastern Siberia, both ORCHIDEE simulation and NDVI show a significant decline of the vegetation response to temperature in northern Europe that is also identified as one of the footprint areas of Barrow by the previous study[18]. Further, the spatial patterns of changes in $R_{\text{NEP-T}}$ (Fig. 3a) and $R_{\text{NPP-T}}$ (Fig. 3b) when NEP is driven by historical precipitation, radiation and temperature are similar to those obtained when NEP is calculated only from

historical temperature (Fig. 3d,e). This suggests that temperature change predominantly explains the simulated decline in local $R_{NPP\text{-}T}$.

Several mechanisms could explain the apparent weakening response of NPP in spring to interannual temperature variations. A first possible mechanism is that winter warming comes with a loss of chilling, so that leaf onset and following spring NPP become less responsive to ST[19]. This phenomenon has been suggested in several observational and experimental studies, involving both woody plants[19] and herbaceous species[20]. To test this mechanism, we performed an additional ORCHIDEE simulation to quantify the relative contribution of changes in chilling days to the decline of $R_{NPP\text{-}T}$ through controlling the historical temperature during the dormancy period (November–April) (simulation S4, see Methods). NEP derived from the difference between simulation S1 (only historical temperature was changed in the ORCHIDEE simulation) and simulation S4 reflects the effect of temperature change during the dormancy period only. Namely, this results in a change in spring NEP in the ORCHIDEE model where the start of the growing season is triggered only after a certain accumulation of heat. We found that changes in chilling days can partly explain a decline of $R_{NPP\text{-}T}$ in eastern Siberia and parts of Alaska (Fig. 3h and Supplementary Fig. 17). Further transport simulation shows that the effect of temperature change during the dormancy period reduced R_{SZC} from −0.73 during the first period to −0.50 during the second period (Fig. 2a). Changes in temperature during the dormancy period (Fig. 3h) could, however, not solely explain the full magnitude of the simulated decline in $R_{NPP\text{-}T}$ (Fig. 3b). Other possible mechanisms that were not specifically tested are the possible limitations of shorter day lengths when the growing season progressively advances earlier into the spring[21], and increasing occurrence of extreme events (such as extreme hot days in eastern Siberia and frost days in northern Europe) (Supplementary Fig. 18a,b)[12]. Further studies are needed to verify these potential mechanisms.

Our results show that the linkage between spring carbon uptake and temperature is not a stable property of northern ecosystems. It demonstrates the value of long-term *in situ* CO_2 records for understanding of the dynamics of the response of the terrestrial carbon balance to climate change. Our results are also relevant to predicting feedbacks between the terrestrial carbon cycle and the global climate system. However, because of the relatively short run of CO_2 observations, it remains uncertain whether the observed decrease in interannual correlation of spring carbon uptake with temperature reflects decadal variability, or a long-term shift in the ecological response of boreal and arctic regions to warming.

Methods

Methods, including statements of data availability and any associated accession codes and references, are available in the online version of this paper.

Received 20 July 2016; accepted 20 March 2017; published online 24 April 2017

References

1. Keeling, C. D., Chin, J. F. S. & Whorf, T. P. Increased activity of northern vegetation inferred from atmospheric CO_2 measurements. *Nature* **382,** 146–149 (1996).
2. Randerson, J. T., Field, C. B., Fung, I. Y. & Tans, P. P. Increases in early season ecosystem uptake explain recent changes in the seasonal cycle of atmospheric CO_2 at high northern latitudes. *Geophys. Res. Lett.* **26,** 2765–2768 (1999).
3. Richardson, A. D. *et al*. Influence of spring and autumn phenological transitions on forest ecosystem productivity. *Phil. Trans. R. Soc. B* **365,** 3227–3246 (2010).
4. Hourdin, F. *et al*. The LMDZ4 general circulation model: climate performance and sensitivity to parametrized physics with emphasis on tropical convection. *Clim. Dynam.* **27,** 787–813 (2006).
5. Krinner, G. *et al*. A dynamic global vegetation model for studies of the coupled atmosphere–biosphere system. *Glob. Biogeochem. Cycles* **19,** GB1015 (2005).
6. Dolman, A. J. *et al*. An estimate of the terrestrial carbon budget of Russia using inventory-based, eddy covariance and inversion methods. *Biogeosciences* **9,** 5323–5340 (2012).
7. McGuire, A. D. *et al*. An assessment of the carbon balance of Arctic tundra: comparisons among observations, process models, and atmospheric inversions. *Biogeosciences* **9,** 3185–3204 (2012).
8. Black, T. A. *et al*. Increased carbon sequestration by a boreal deciduous forest in years with a warm spring. *Geophys. Res. Lett.* **27,** 1271–1274 (2000).
9. Barichivich, J. *et al*. Large-scale variations in the vegetation growing season and annual cycle of atmospheric CO_2 at high northern latitudes from 1950 to 2011. *Glob. Change Biol.* **19,** 3167–3183 (2013).
10. D'Arrigo, R. D. *et al*. Thresholds for warming-induced growth decline at elevational tree line in the Yukon Territory, Canada. *Glob. Biogeochem. Cycles* **18,** GB3021 (2004).
11. Angert, A. *et al*. Drier summers cancel out the CO_2 uptake enhancement induced by warmer springs. *Proc. Natl Acad. Sci. USA* **102,** 10823–10827 (2005).
12. Piao, S. *et al*. Evidence for a weaking relationship between interannual temperature variability and northern vegetation activity. *Nat. Commun.* **5,** 5018 (2014).
13. Graven, H. D. *et al*. Enhanced seasonal exchange of CO_2 by northern ecosystems since 1960. *Science* **341,** 1085–1089 (2013).
14. Piao, S. *et al*. Net carbon dioxide losses of northern ecosystems in response to autumn warming. *Nature* **451,** 49–52 (2008).
15. Takala, M. *et al*. Estimating Northern Hemisphere snow water equivalent for climate research through assimilation of space-borne radiometer and ground-based measurements. *Remote Sens. Environ.* **115,** 3517–3529 (2011).
16. Viovy, N. & Ciais, P. *CRUNCEP data set for 1901–2012 Tech. Rep. V. 4* (Laboratoire des Sciences du Climat et de l'Environnement, 2014); https://www.earthsystemgrid.org/browse/viewActivity.html?activityId=ff9d6ffb-f0b9-11e2-aa24-00c0f03d5b7c
17. Goulden, M. L. *et al*. Sensitivity of boreal forest carbon balance to soil thaw. *Science* **279,** 214–217 (1998).
18. Kaminski, T., Giering, R. & Heimann, M. Sensitivity of the seasonal cycle of CO_2 at remote monitoring stations with respect to seasonal surface exchange fluxes determined with the adjoint of an atmospheric transport model. *Phys. Chem. Earth* **21,** 457–462 (1996).
19. Fu, Y. H. *et al*. Declining global warming effects on the phenology of spring leaf unfolding. *Nature* **526,** 104–107 (2015).
20. Yu, H., Luedeling, E. & Xu, J. Winter and spring warming result in delayed spring phenology on the Tibetan Plateau. *Proc. Natl Acad. Sci. USA* **107,** 22151–22156 (2010).
21. Stine, A. R. & Huybers, P. Arctic tree rings as recorders of variations in light availability. *Nat. Commun.* **5,** 3836 (2014).

Acknowledgements

This study was supported by the National Natural Science Foundation of China (41530528), the International Partnership Program of Chinese Academy of Sciences (Grant No. 131C11KYSB20160061), the BELSPO STEREO project ECOPROPHET (SR00334), the 111 Project (B14001), and National Youth Top-notch Talent Support Program in China. P.C., I.A.J. and J.P. acknowledge support from the European Research Council through Synergy grant ERC-2013-SyG-610028 'P-IMBALANCE'. Analysis of FLEXPART was conducted within the LATICE project at the University of Oslo. J.Mao and X.Shi are supported by the Biogeochemistry-Climate Feedbacks Scientific Focus Area project funded through the Regional and Global Climate Modeling Program in the Climate and Environmental Sciences Division (CESD) of the Biological and Environmental Research (BER) Program in the US Department of Energy Office of Science. Oak Ridge National Laboratory is managed by UT-BATTELLE for DOE under contract DE-AC05-00OR22725.

Author contributions

S.Piao designed the research; Z.L., T.W. and P.P.T. performed measurements of CO_2 data analysis; S.Peng, T.W. and Z.L. performed ORCHIDEE modelling and transport analysis; F.C., J.F.B. and A.S. performed footprint analysis; S.Piao drafted the paper; and all authors contributed to the interpretation of the results and to the text.

Additional information

Supplementary information is available in the online version of the paper. Reprints and permissions information is available online at www.nature.com/reprints. Publisher's note: Springer Nature remains neutral with regard to jurisdictional claims in published maps and institutional affiliations. Correspondence and requests for materials should be addressed to S.Piao.

Competing financial interests

The authors declare no competing financial interests.

Methods

Atmospheric CO_2 concentration data. Daily atmospheric CO_2 concentration records constructed from surface *in situ* continuous measurements at Point Barrow, Alaska, were obtained from the National Oceanic and Atmospheric Administration (NOAA) Earth System Research Laboratory archive[22] for the period of 1979–2012. To separate the seasonal cycle from the long-term increase in CO_2, the daily data was firstly fitted with a function consisting of a quadratic polynomial for the long-term trend and four harmonics for the annual cycle[23]. The residuals from this function fit are then obtained. A smooth curve was obtained by digitally removing the short-term variation from the residuals using 1.5 month (or 1.0 month, see Supplementary Fig. 9) full-width half-maximum value (FWHM) averaging filter and then adding the filtered residuals to the fitted function. A de-seasonalized long-term trend was obtained by digitally filtering the residuals using a 390-day FWHM averaging filter and then adding the filtered residuals to the quadratic polynomial long-term trend. The difference between the smooth curve and the de-seasonalized long-term trend is then used to represent the detrended seasonal CO_2 curve. Note that any data lying outside 5 (or 3, 2.5, see Supplementary Fig. 9) standard deviations of the residuals between the original data and the smooth curve were regarded as outliers and discarded from the original daily time series[24]. This procedure was repeated until no outliers were identified. The spring (downward) zero-crossing date (SZC) for each year was then determined as the day of the year (DOY) when the sign of the seasonal CO_2 excursion from the annual mean trend changed from positive to negative (Supplementary Fig. 1). Based on the detrended seasonal CO_2 curve, the mean estimate of SZC over the period of 1979–2012 at Barrow is around DOY 180 with a year-to-year variability of 3.5 days (DOY range from 173 to 188). The seasonal maximum of atmospheric CO_2 occurs during the period from late April to early May. Defining spring as the months of May and June, the change in CO_2 over this spring period (hereafter SCC) was also computed for each year from the detrended seasonal CO_2 cycle (Supplementary Fig. 1). We also used records of weekly atmospheric CO_2 concentration records, based on either surface *in situ* continuous measurements or surface flask samples, from the NOAA Earth System Research Laboratory[25] at Barrow (Supplementary Fig. 10) and derived similar results. We also used weekly atmospheric CO_2 concentration at the surface based on flask samples at the Alaskan Point Cold Bay and Norwegian Ocean Station M site[25] that have relatively longer observations (34 years and 29 years, respectively) (Supplementary Fig. 12). We did not perform outlier detection for weekly data because these CO_2 concentration records had already been processed (smoothed, interpolated, and extrapolated) in the GLOBVIEW-CO_2 product to address issues of temporal discontinuity and data sparseness in atmospheric observations.

We adopted two different approaches to identify the areas that mainly affect the change in spring CO_2 concentration at Barrow (hereafter as spring footprint area). The first approach to define spring footprint area is through using the adjoint code of the LMDZ atmospheric transport model[26] to calculate the specific sensitivity of the Barrow CO_2 measurements to NEP in the Northern Hemisphere. This adjoint code applies the chain rule to all partial derivatives within LMDZ and therefore allows us to compute exact partial derivatives of concentration measurements with respect to NEP everywhere over the globe and at anytime before a given CO_2 observation at Barrow. The derivatives in units of concentration (ppm) per unit flux (kg C m^{-2} h^{-1}) were computed for measurements made at the Point Barrow station on the 28th day of each month at 19:00 UTC, a typical flask sampling time at this station, and for all global grid-point fluxes at the daily scale since the start of the month. We then averaged the derivatives for the months from March to June in each year between 1979 and 2012 to get an average footprint of the measurements during spring (Supplementary Fig. 6a–c).

The second method to define spring footprint area is based on the Lagrangian particle dispersion model FLEXPART (version 8.2). FLEXPART simulates atmospheric transport using wind fields from global forecast models to determine source to receptor pathways of air masses[27], and the simulations are available for the period of 1985–2009 inclusive, at 3-hourly resolution. For our simulations, the model was forced with wind field data from the European Centre for Medium-Range Weather Forecasts (ECMWF). Backward in time, or so-called 'retroplume'[28], calculations were made to provide a footprint map of the Barrow measurements. Every 3 h, 40,000 particles are released from the measurement site location and followed backwards in time for 20 days. Integrating time at the lowest model output layer (0–100 m) over the 20-day period provides a map of Potential Emission Sensitivity for the measurement site. Post-processing of the results was conducted to evaluate the variability of the mean footprint source region for Barrow. The 3-hourly results were averaged into monthly values from March to June, and subsequently into spring values (Supplementary Fig. 6d–f).

Climate data. Monthly climate data (temperature, precipitation and cloud cover) at a spatial resolution of 0.5° from 1901 to 2012 were taken from the University of East Anglia's Climate Research Unit CRU TS 3.22 data set[29]. We also applied another two climate data sets (Climatic Research Unit–National Centers for Environmental Prediction (http://dods.extra.cea.fr/data/p529viov/cruncep) and Watch Forcing Data methodology applied to ERA-Interim data (http://www.eu-watch.org/gfx_content/documents/README-WFDEI.pdf)), and returned very similar results (Supplementary Fig. 8). Snow water equivalent was derived from the European Space Agency's Global Snow Monitoring for Climate Research (GlobSnow) product that is generated by combining satellite data with ground measurements of snow depth[15].

Satellite Normalized Difference Vegetation Index (NDVI) data. We used the third Normalized Difference Vegetation Index (NDVI3g) data product generated from Advanced Very High Resolution Radiometer (AVHRR) data by the Global Inventory Monitoring and Modeling Studies (GIMMS)[30]. AVHRR NDVI3g has a spatial resolution of 8 km and a repeat cycle of 15 days for 1982–2011. This product has been carefully assembled from different AVHRR sensors, removing several detrimental effects, such as calibration loss, orbit drift, and volcanic eruption.

Terrestrial carbon-cycle model. ORCHIDEE (ORganizing Carbon and Hydrology In Dynamic Ecosystems) is a process-based model that calculates the fluxes of CO_2, H_2O and heat between the atmosphere and the land surface on a half-hourly basis, and the variations in the water and carbon pools on a daily basis[5]. Here, we used the version that was used in the IPCC AR5. ORCHIDEE simulates carbon-cycle processes such as half-hourly photosynthesis, as well as carbon allocation, litter decomposition, soil carbon dynamics, maintenance and growth respiration, and phenology at the daily time step. ORCHIDEE has been widely used for investigating terrestrial carbon-cycle dynamics and their responses to climate variations. In the phenology module of ORCHIDEE, a certain amount of heat is needed for boreal vegetation to initiate leaf unfolding in spring. This heat requirement is estimated by growing degree days (GDD)[31], which is negatively correlated with chilling days during the dormancy period. As shown in Supplementary Fig. 19, ORCHIDEE generally captured the spatial and temporal characteristics of satellite-based spring phenology over the boreal region[32].

We ran the ORCHIDEE model until the carbon pools reached equilibrium after about 1000 years. We used a resolution of 0.5°, with 1901 climate data and the 1860 atmospheric CO_2 concentration of 286.05 ppm. The model was then run to 1978 with a transient climate and the corresponding observed atmospheric CO_2 concentration during that period. Note that because there are no climate data during 1860–1900, the transient 1901–1910 climate was recycled for 1860–1900. The historical climate forcing used in ORCHIDEE was from the CRU–NCEP data set[16]. For years 1979–2012, we performed four different simulations (S1, S2, S3 and S4). In simulation S1, only historical temperature was changed. In simulation S2, only historical temperature and precipitation were changed. In simulation S3, atmospheric CO_2 and all historical climatic factors were changed. In simulation S4, only historical temperature from May to October was changed through simply treating November–April as the dormancy period.

Air–sea CO_2 fluxes. A biogeochemical model PlankTOM5 combined with a global ocean general circulation model NEMO (NEMO-PlankTOM5) were used to simulate the physical, chemical and biological processes that affect the surface ocean CO_2 concentration and thus the air–sea CO_2 exchange[33,34]. The PlankTOM5 model was forced by inputs of ions and compounds from river, sediment and dust[35,36]. The NEMO model was driven by daily wind and precipitation from the NCEP reanalysis[37]. Further details are given by ref. 33.

Atmospheric transport model. We used LMDZ4, a 3D atmospheric tracer transport model from the Laboratoire de Météorologie Dynamique[4], nudged with horizontal winds from the ECMWF reanalysis, to transform NEP from ORCHIDEE into a point estimate of CO_2 concentration at Barrow station. To separate the effects of transport and terrestrial carbon fluxes on the SZC and SCC signal, we performed several transport simulations with year-to-year varying winds (see Table 1). The first one (referred to as CFTT simulation) used periodical NEP of 1979 from ORCHIDEE simulation S3. The second one (referred to as TFTT simulation) used the year-to-year varying NEP fluxes calculated during the period 1979–2012 by simulation S3. The third simulation is similar to TFTT, but used year-to-year varying NEP fluxes for only north of 50° N (TFTT-B). The contribution of year-to-year varying fluxes to the variability in SZC and SCC is assessed by the difference in simulated atmospheric CO_2 between the first and the second simulations, which we refer to as the TFCT simulation. The difference between TFTT-B and CFTT is used to give the contribution of boreal fluxes to the variability in SZC and SCC (referred to as TFCT-B). Two daily NEP outputs from ORCHIDEE (S1 and S2) over the period 1979–2012 were fed into the transport model to derive their respective daily CO_2 concentrations at Barrow station. To further separate the relative roles of NPP and HR, we also performed two additional transport simulations using daily NEP calculated from year-to-year varying NPP and periodical HR of 1979 based on the S3 simulation, and from year-to-year varying HR and periodical NPP of 1979 based on the S3 simulation. Using a similar method of estimation as used in the TFCT-B simulation, we calculated the contribution of temperature change (referred to as TFCT-T simulation), both temperature and precipitation changes (referred to as TFCT-TP simulation), year-to-year varying NPP fluxes (referred to as TFCT-NPP

simulation), and year-to-year varying HR fluxes (referred to as TFCT-HR simulation) over land north of 50° N (see Table 1). Additionally, we performed a transport simulation TFTT-D using the same strategy as TFTT-T, but NEP derived from simulation S4 (only historical temperature from May to October was changed in the ORCHIDEE simulation). The difference between transport simulations TFTT-T and TFTT-D (denoted as TFCT-D) is then used to estimate the contribution of changes in temperature during the dormancy period (November–April) to the SZC and SCC signal. It should be noted that air–sea CO_2 fluxes in all above simulations were constant. To understand the potential ocean contribution, we added another transport simulation (CFTT-Ocean), which is similar to CFTT but transports year-to-year varying air–sea carbon flux from ocean models. The effect of air–sea flux changes is then evaluated from the difference of the two simulations (CFTT-Ocean minus CFTT).

Analysis. Spring vegetation activity is closely linked to the temperatures in the preceding months. All variables are first detrended in the statistical correlation analysis since we focus on the interannual relationship between spring carbon uptake and temperature. Then we determined the length of the preseason whose average temperature had the largest influence on SZC and SCC by calculating the partial correlation coefficients of SZC and SCC with temperature during the 0, 1, 2, 3 . . . 7 months before June (SZC over the period of 1979–2012 at Barrow is around DOY 180). We found that the average temperature from March to June (ST) was most strongly negatively correlated with SZC (highest positive interannual correlation with SCC) at Barrow for 1979–2012; we therefore used the average temperature during these months (Supplementary Fig. 3). Then we calculated the partial correlation coefficient of SZC and SCC with ST for the earliest 17 years (1979–1995) and the more recent 17 years (1996–2012), through randomly selecting 14 years among the corresponding period. A two-sample t-test was conducted to determine whether there is a statistically significant difference in R_{SZC} (or R_{SCC}) between the first (1979–1995) and second (1996–2012) half-study period. Using a similar method, for each randomly selected period (for example, 14 of 17 years during the first half-study period (1979–1995)), we also defined preseason (the period before June for which the negative interannual correlation between SZC and temperature (positive interannual correlation for SCC) was highest) to further assess the robustness of the inferred decline of R_{SZC} and R_{SCC} over the past three decades (Supplementary Fig. 9).

We performed partial correlation analyses between SZC (SCC) and ST (R_{SZC} and R_{SCC}) after statistically controlling for interannual variation in precipitation and cloud cover during the period from March to June. The partial correlation coefficient R_{SZC} (R_{SCC}) is computed as the interannual correlation between the residuals calculated after regressing SZC (SCC) on precipitation and cloud cover and those after regressing ST on precipitation and cloud cover. The interannual sensitivity of SZC (γ_{SZC}) to ST variation was computed as the slope of the regression of ST in a multiple linear regression of SZC against temperature, precipitation and cloud cover during the period from March to June. We apply the same approach to calculate interannual sensitivity of SCC (γ_{SCC}) to ST variation. Temperature, precipitation and cloud cover were computed as the spatial average over the vegetated land area north of 50° N. We also used climate variables computed as the spatial average weighted by the sensitivities (surface flux sensitivity from LMDZ and potential emission sensitivity from FLEXPART) over the vegetated land area within the multi-year mean spring footprint area. The vegetated land area is defined as grid points where the average of annual mean NDVI over the period of 1982–2011 is larger than 0.1. All variables were linearly detrended over the study period before the partial correlation and regression statistical analyses were performed. Similar results were also derived from analyses without detrending variables (Supplementary Fig. 20).

To investigate whether a different magnitude of variation in spring carbon uptake and temperature during the two time periods would change our results, we calculated the standard deviation (sd) of SZC/SCC/ST for both periods. As shown in Supplementary Fig. 21a, the sd of SZC during the first period is even lower than that during the last period. For SCC and ST, the sd during the first 17 years is higher than that during the last 17 years (Supplementary Fig. 21b,c). We should be extremely careful in interpreting this result, since the observed large variability of SCC and ST in the first 17 years is heavily influenced by the year 1990 with a high anomaly (Supplementary Fig. 2). If the year 1990 was excluded, the sd of SCC and ST in the first 17 years are even smaller than those in the last 17 years (Supplementary Fig. 21b,c). Nevertheless, the significant partial correlation between SZC and ST for the first 17 years is still observed when the year 1990 is removed (Supplementary Fig. 21d, $R_{SZC} = -0.76 \pm 0.13$, $P = 0.001$). The same analysis using SCC instead of SZC yields similar results (Supplementary Fig. 21e, $R_{SCC} = 0.52 \pm 0.24$, $P = 0.054$). Therefore, the different magnitude of variation in ST, SZC and SCC between the two periods should not be regarded as an influencing factor in explaining the recent decline in R_{SZC} and R_{SCC}.

To investigate the effect of frost events after early spring leaf-out on the interannual correlation between spring carbon uptake and temperature, we calculated frost days for each grid cell north of 50° N. The frost days were defined as the sum of days when daily minimum air temperature was below 0° from the start of the growing season (SOS) to the summer solstice. Here we determined SOS by taking the ensemble mean of the results from four SOS estimation methods[32,38] (HANTS-Maximum, Polyfit-Maximum, double logistic and piecewise logistic) applied to satellite NDVI data.

Data availability. The atmospheric CO_2 concentration data that support the findings of this study are available in National Oceanic and Atmospheric Administration (NOAA), Earth System Research Laboratory (ESRL), Global Monitoring Division (GMD): Boulder, Colorado, USA[22] (ftp://aftp.cmdl.noaa.gov/data/trace_gases/co2/in-situ/surface/brw/co2_brw_surface-insitu_1_ccgg_DailyData.txt). Climate data used for calculating temperature sensitivity were obtained from three publicly available sources—Climate Research Unit (http://catalogue.ceda.ac.uk/uuid/4a6d071383976a5fb24b5b42e28cf28f), Climatic Research Unit–National Centers for Environmental Prediction (https://www.earthsystemgrid.org/browse/viewActivity.html?activityId=ff9d6ffb-f0b9-11e2-aa24-00c0f03d5b7c) and Watch Forcing Data methodology applied to ERA-Interim data (http://www.eu-watch.org/gfx_content/documents/README-WFDEI.pdf). The ORCHIDEE-LMDZ simulation results are available from the corresponding author upon request.

References

22. Thoning, K. W., Kitzis, D. R. & Crotwell, A. *Atmospheric Carbon Dioxide Dry Air Mole Fractions from Quasi-Continuous Measurements at Barrow, Alaska* (NOAA ESRL Global Monitoring Division, 2014); ftp://aftp.cmdl.noaa.gov/data/trace_gases/co2/in-situ/surface/brw/co2_brw_surface-insitu_1_ccgg_DailyData.txt
23. Thoning, K. W., Tans, P. P. & Komhyr, W. D. Atmospheric carbon dioxide at Mauna Loa observatory. 2. Analysis of the NOAA GMCC data, 1974–1985. *J. Geophys. Res.* **94,** 8549–8565 (1989).
24. Harris, J. M. *et al*. An interpretation of trace gas correlations during Barrow, Alaska, winter dark periods, 1986–1997. *J. Geophys. Res.* **105,** 17267–17278 (2000).
25. Cooperative Global Atmospheric Data Integration Project *Multi-Laboratory Compilation of Synchronized and Gap-Filled Atmospheric Carbon Dioxide Records for the Period 1979–2012* (*obspack_co2_1_GLOBALVIEW-CO_2_2013_v1.0.4_2013-2-23*)(NOAA Global Monitoring Division, 2013); http://dx.doi.org/10.3334/OBSPACK/1002
26. Chevallier, F. *et al*. Inferring CO_2 sources and sinks from satellite observations: method and application to TOVS data. *J. Geophys. Res.* **110,** D24309 (2005).
27. Stohl, A., Forster, C., Frank, A., Seibert, P. & Wotawa, G. The Lagrangian particle dispersion model FLEXPART version 6.2. *Atmos. Chem. Phys.* **5,** 2461–2474 (2005).
28. Stohl, A., Forster, C. & Eckhardt, S. *et al*. A backward modeling study of intercontinental pollution transport using aircraft measurements. *J. Geophys. Res.* **108,** 4370 (2003).
29. Mitchell, T. D. & Jones, P. D. An improved method of constructing a database of monthly climate observations and associated high-resolution grids. *Int. J. Climatol.* **25,** 693–712 (2005).
30. Tucker, C. J. *et al*. An extended AVHRR 8-km NDVI dataset compatible with MODIS and SPOT vegetation NDVI data. *Int. J. Remote Sens.* **26,** 4485–4498 (2005).
31. Piao, S., Friedlingstein, P., Ciais, P., Viovy, N. & Demarty, J. Growing season extension and its impact on terrestrial carbon cycle in the Northern Hemisphere over the past 2 decades. *Glob. Biogeochem. Cycles* **21,** GB3018 (2007).
32. Wang, X. *et al*. Has the advancing onset of spring vegetation green-up slowed down or changed abruptly over the last three decades? *Glob. Ecol. Biogeogr.* **24,** 621–631 (2015).
33. Buitenhuis, E. T., Rivkin, R. B., Sailley, S. & Le Quéré, C. Biogeochemical fluxes through microzooplankton. *Glob. Biogeochem. Cycles* **24,** GB4015 (2010).
34. Le Quéré, C. *et al*. Global carbon budget 2015. *Earth Syst. Sci. Data* **7,** 349–396 (2015).
35. Cotrim da Cunha, L., Buitenhuis, E. T., Le Quéré, C., Giraud, X. & Ludwig, W. Potential impact of changes in river nutrient supply on global ocean biogeochemistry. *Glob. Biogeochem. Cycles* **21,** GB4007 (2007).
36. Aumont, O., Maier-Reimer, E., Blain, S. & Monfray, P. An ecosystem model of the global ocean including Fe, Si, P colimitations. *Glob. Biogeochem. Cycles* **17,** 1060 (2003).
37. Kalnay, E. *et al*. The NCEP/NCAR 40-year reanalysis project. *Bull. Am. Meteorol. Soc.* **77,** 437–471 (1996).
38. Liu, Q. *et al*. Temperature, precipitation, and insolation effects on autumn vegetation phenology in temperate China. *Glob. Change Biol.* **22,** 644–655 (2016).